www.acsnano.org

Thermal Activation of Anti-Stokes Photoluminescence in CsPbBr₃ Perovskite Nanocrystals: The Role of Surface Polaron **States**

Kylie M. Lytle, Emma L. Brass, Benjamin J. Roman, and Matthew T. Sheldon*



Downloaded via UNIV OF CALIFORNIA IRVINE on March 8, 2025 at 21:39:06 (UTC). See https://pubs.acs.org/sharingguidelines for options on how to legitimately share published articles.

Cite This: ACS Nano 2024, 18, 18457-18464



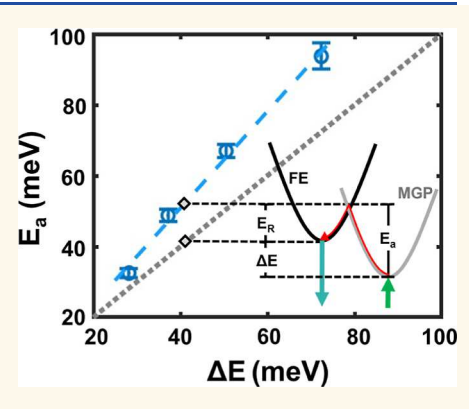
ACCESS I

III Metrics & More

Article Recommendations

Supporting Information

ABSTRACT: Optically driven cooling of a material, or optical refrigeration, is possible when optical up-conversion via anti-Stokes photoluminescence (ASPL) is achieved with near-unity quantum yield. The recent demonstration of optical cooling of CsPbBr₃ perovskite nanocrystals (NCs) has provided a path forward in the development of semiconductor-based optical refrigeration strategies. However, the mechanism of ASPL in CsPbBr₃ NCs is not yet settled, and the prospects for cooling technologies strongly depend on details of the mechanism. By analyzing the Arrhenius behavior of ASPL in CsPbBr₃ NCs, we investigated the relationship between the average energy gained per photon during up conversion, ΔE , and the thermal activation energy, E_a . We find that E_a is systematically larger than ΔE , and that E_a increases for larger ΔE . We suggest that the additional energetic cost is due to a rearrangement of the crystal lattice as charge carriers pass from surface localized, structurally distinct sub-gap polaron states to the free exciton state



during up-conversion. Our interpretation is further corroborated by quantifying the impact of ligand coverage on the NC surface. These findings help inform the development of CsPbBr₃ NCs for applications in optical refrigeration.

KEYWORDS: CsPbBr3 perovskite nanocrystal, optical cooling, polaron, anti-Stokes photoluminescence, up-conversion

CsPbBr₃ perovskite nanocrystals (CsPbBr₃ NCs) are among the first semiconductor materials known to undergo optical cooling.1 The mechanism of cooling is based on anti-Stokes photoluminescence (ASPL), which is luminescent emission of a photon at greater energy than the energy of the photon that was absorbed. The energy gain of the up-converted photon due to ASPL is provided by scavenged thermal energy from the luminescent material. High photoluminescence quantum yield (PLQY), that is maintained during below-gap excitation is critical for cooling to occur, as it ensures that the energy radiated by the up-converted photons surpasses the heat introduced by non-radiative decay.

Optical cooling was first observed in rare-earth doped glasses (REG) and since there have been claims of optical cooling in some organic dyes and semiconductor nanostructures, though some of these claims have been questioned. 12-15 The low temperature limit of optical cooling is dependent on the electronic and vibrational state structure that facilitates ASPL. In REG the Stark Effect creates a manifold of both ground and excited electronic states. Low energy photons excite electrons from the highest energy ground state to the lowest energy excited state. Then after thermal equilibration within the

manifold, electrons relax to the ground state, emitting photons at greater energy than was absorbed.^{2-4,16} Similarly, ASPL in organic dyes relies on excitation from vibrationally excited ground states, followed by optical emission when electrons relax into a ground state with lower vibrational activation. 5-Because these mechanisms of ASPL are mediated by thermally activated electronic ground states, optical cooling in REGs and organic dyes is limited to temperatures for which these states are populated.

Semiconductor materials are hypothesized to achieve ASPL via a distinct mechanism. Photocarriers with energy less than the thermally broadened band-edge emission energy are excited from the valence band to the bottom of the conduction band. Emission at a higher energy may be achieved by thermal

Received: March 14, 2024 Revised: June 25, 2024 Accepted: June 27, 2024 Published: July 5, 2024





equilibration of carriers within the conduction band before optical recombination. $^{17-19}$ Alternatively, electrons can be excited from the valence band to just below the band edge. Excitation into the conduction band is possible via phonon assisted absorption or via thermal equilibration within a subgap state. 20-22 Because ASPL in semiconductors does not rely on excitation from thermally activated ground state—that is, excitation from the valence band is possible even at absolute zero—it is theorized that semiconductors can be optically cooled to much lower cryogenic temperatures than REGs or organic dyes. 17,19 The hypothetically lower temperature that can be achieved, in combination with the variety of established optoelectronic technologies based on semiconductor device platforms, entails that optical cooling in semiconductors has been a long-sought goal. A major challenge, despite the sufficiently high internal quantum efficiency of many photoluminescent semiconductors, is that total internal reflection traps ASPL within the solid, making it extremely challenging to achieve the external PLQY necessary for cooling. 19 Only recently has optical cooling been observed in semiconductor nanostructures, 8,9 including CsPbBr₃ NCs. The subwavelength size of these NCs entails that total internal reflection does not occur, and near unity PLQY is routinely achieved for colloidal suspensions. Hence, CsPbBr₃ NCs are a promising road forward in the development of optical cooling technology.^{23,24}

Although optical cooling has been demonstrated in CsPbBr₃ NCs, there remains a lack of understanding regarding the ASPL mechanism, so the theoretical cooling limits and possible paths toward optimization are unclear. Initial models of ASPL in CsPbBr₃ and other semiconductor nanostructures that show ASPL have assumed that sub-gap optical excitation promotes photocarriers to a mid-gap state, followed by thermalization to the conduction or valence band edge that is mediated via electron-phonon coupling.^{25,26} The energy gains possible during ASPL are greater than any single phonon mode that has been measured in CsPbBr₃ NCs so it is believed to be a multiphonon process. 27,28 The precise nature of the sub-gap state which assists ASPL is disputed. Though there is evidence that shallow defect states or surface states associated with dangling bonds, energetically within the band gap, can promote ASPL in similar material systems, 20,21,26,29,30 our previous research has shown that ASPL efficiency increased by as much as a factor of 3 when CsPbBr₃ NCs were treated postsynthetically to reduce trap states and defects.³¹ Given that ASPL is observed even for CsPbBr₃ NCs that exhibit nearunity PLQY (>98%) alternative mechanistic pictures have been proposed that do not rely on defects that also promote non-radiative recombination. Further, in CsPbBr₃ NCs we observe no spectroscopic structure in the absorption edge or ASPL yield, implying the existence of discrete sub-gap states with well-defined energy, see Figure 1B below. Alternatively, mid-gap polaron states (MGP), hybrid electron-phonon states caused by distortions in the crystal lattice that modify the energy of a photocarrier, have been proposed as the relevant sub-gap state. The relevant MGPs may result from thermally induced lattice fluctuations, or from photoexcitation in the form of self-trapped excitons (STEs). 22,32,33 However, STEs rely on above-gap excitation to induce a lattice distortion, and this is inconsistent with up-conversion. In comparison, thermally induced lattice fluctuations induce MGPs with an exponentially decreasing density of states below the band edge, and the resulting perturbation to the intrinsic electronic

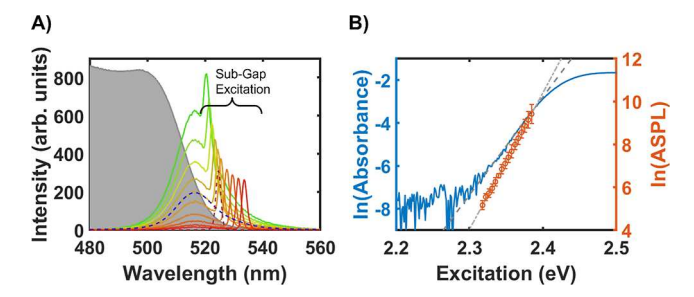


Figure 1. (A) ASPL spectra with different sub-gap excitation wavelengths. Scattering from the excitation source can be seen as narrow peaks which are labeled. The absorbance curve of CsPbBr₃ NCs is shown in solid gray for reference. The dashed blue line shows an example fit for the contribution from the ASPL emission, and the dashed red line shows an example fit for the contribution from the excitation source. (B) Comparison of the Urbach tail region and the integrated ASPL intensity at different excitation energies. The log scale of absorbance is shown in the solid blue line with a dashed dark gray line indicating the linear fit and the log scale of integrated ASPL intensity is shown in orange circles, with a double-dashed light gray line indicating the linear fit.

structure is pronounced in lead halide perovskites due to the relatively soft ionic lattice. ^{32–36}

We sought to gain greater insight into the up-conversion mechanism through a study of the thermal activation of ASPL. As we detail below, the yield of ASPL exhibits very clear Arrhenius behavior, allowing for determination of an activation energy, E_a , associated with the up-conversion process. The activation energy is determined by the rate limiting step of the ASPL mechanism. Therefore, an analysis of E_a can give insight into the energetic requirements of up-conversion that may not be apparent in the absorption or emission spectra, if these spectra are only diagnostic of the initial and final state in the mechanism, respectively. We measured the activation energy of ASPL for colloidal solutions of CsPbBr₃ NCs while varying the sub-gap excitation energy, in order to analyze the dependence on the up-converted energy gain, ΔE . We found that E_a is not equivalent to ΔE , and that there is an additional energy cost beyond ΔE which increases linearly as ΔE increases. This trend is consistent with an energy associated with atomic rearrangement in the NC lattice (E_R) that is required for photocarriers to pass from a MGP state to the free exciton (FE) state. We also found the ligand coverage of the NCs has a large impact on E_R , further supporting a mechanistic picture in terms of thermally activated structural rearrangements on the NC surface.

RESULTS AND DISCUSSION

ASPL in CsPbBr₃ Perovskite NCs. The CsPbBr₃ NCs studied in this paper are approximately 8.7 ± 2.1 nm on an edge, and range in emission from 511 to 515 nm (see Figures S1 and S2). As is expected for NC of this size, the absorbance spectra do not show evidence of quantum confinement. Studies from our laboratory and others show that the yield of ASPL from CsPbBr₃ NCs displays a linear power law over many orders of magnitude, indicating that up-conversion is a single photon process, when excited as far as 95 meV below the band edge (see Figure S3 and Table S1). Powever, when excitation is further red-shifted, the much smaller cross section for two-photon absorption becomes relatively significant, so that the power law for up-converted photoluminescence gains superlinear character. As reported by

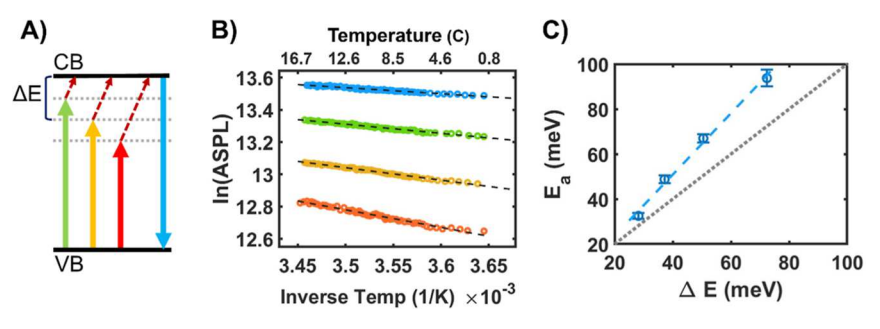


Figure 2. (A) Energy level schematic of ASPL mechanism illustrating how different excitation energy leads to different up-conversion energy gains, ΔE . (B) Arrhenius plots of the thermal activation of ASPL intensity with different ΔE s. The blue, green, yellow, and orange traces represent data where ΔE is 28, 37, 50, and 72 meV, respectively. The lines of best fit, shown as dashed black lines, represent the best fit to the linear Arrhenius equation: $\ln(\text{ASPL}) = \left(\frac{-E_a}{k_b}\right)\left(\frac{1}{T}\right) + \ln(C)$. The data have been offset along the y-axis for ease of viewing. (C) The activation energy, E_a , versus the up-conversion energy gain, ΔE , as shown in (B). The data points are shown in blue, with line of best fit shown in dashed blue. The gray dashed line represents the hypothetical scenario where $E_a = \Delta E$.

Grandados del Aguila et al., and observed in studies in our laboratory (see Figure S4), two photon up-conversion starts to become significant when exciting between 150 and 200 meV below-gap. 27,28 When sub-gap excitation decreases in energy there is an exponential decrease in ASPL intensity (see Figure 1A). For excitation energy with small detuning, where twophoton process does not contribute, throughout the spectral region known as the Urbach tail, it is reasonable to expect that the spectral-dependent decrease in ASPL intensity may simply be proportional to the exponential decrease in absorbance. This Urbach tail region corresponds to the temperature dependent broadening of the band edge electronic states, and it can be caused by crystal strain, defects, phonon coupling, and NC size polydispersity. The extent of this energy broadening can be quantified as the Urbach energy, E_w using the expression $\alpha \sim \exp\left(\frac{E}{E_u}\right)$, where E is the excitation energy, and α is absorbance.^{38–40} When the band edge absorbance and the spectrally integrated ASPL yield are overlaid on a log plot, it becomes clear that the exponential decrease in ASPL yield is not proportional to the Urbach tail (see Figure 1B). Both trends can be fit to the expression for $E_{\rm u}$, with the fit to the ASPL intensity of $E_{\rm u}^{\rm ASPL} = 15.7 \pm 0.1 \, {\rm meV}$ and the fit to the absorption edge of $E_{\rm u}^{\alpha}=21.9\pm0.3$ meV for the measured sample. Variations in $E_{\rm u}^{\rm ASPL}$ and $E_{\rm u}^{\alpha}$ values between different NC synthesizes as well as trends in $E^{\alpha}_{\rm u}$ with different NC sizes reflected in photoluminescence emission peak can be found in the Figures S5 and S6. Despite variations in explicit E_u^{ASPL} and $E_{\rm u}^{\alpha}$ values the difference between them, with $E_{\rm u}^{\alpha}$ consistently being greater, remains apparent. The discrepancy between the band edge absorbance and ASPL intensity throughout the Urbach tail spectral region may suggest the role of intermediate steps between optical absorption and ASPL emission. These trends further indicate the complex spectral dependence of quantum yield for ASPL. This data appears to be consistent with observations made by Zhang et al. of decreases in the efficiency of up-conversion as excitation is detuned from the band edge of surface-deposited CsPbBr₃ NC samples. 27 Additionally, the smooth exponential decay in ASPL suggests a continuum of sub-gap states, as opposed to a single discrete electronic state assisting in up-conversion.

Up-Conversion Energy Gain (ΔE) and Activation Energy (E_a) . The ASPL emission from samples of CsPbBr₃ NCs occurs at the same wavelength as the band-edge recombination observed during above-gap excitation (see

Figure S7),³⁷ and the ASPL emission energy is constant as excitation energy is detuned to lower energy (see Figure 1A). The energy gain from up-conversion, ΔE , is defined as the difference between the average energy of the absorbed photons and the emitted photons during the ASPL process, and it is equivalent to the anti-Stokes shift. This value is significant in optical cooling as it describes the quantity of energy that is removed from the system with each up-conversion event. As ASPL emission of CsPbBr₃ NCs is independent of the energy of the sub-gap excitation, ΔE can be increased by red-shifting the energy of excitation (see Figure 2A). A larger ΔE value means that more energy is removed from the system with each ASPL up-conversion event, however the trade-off is that higher excitation powers are needed to offset for the exponential decrease in absorbance as excitation is red-shifted below the band gap.

Over temperature ranges where other temperature-dependent processes such as crystalline phase transitions or other thermally activated non-radiative losses do not play a significant role, 22,41,42 the increase in ASPL intensity with temperature exhibits Arrhenius behavior. Therefore, it is possible to analyze the yield of ASPL in terms of an energy of activation, $E_{\rm a}$, which is a measure of the thermal energy required to overcome the rate-limiting step during ASPL, using the linear Arrhenius equation

$$\ln(ASPL) = \frac{-E_a}{k_b} \left(\frac{1}{T}\right) + \ln(C)$$
(1)

Here, ASPL is the integrated intensity of ASPL at temperature T (in Kelvin), $k_{\rm b}$ is Boltzmann's constant, and C is the Arrhenius pre-exponential factor. Notably the calibration of the Arrhenius behavior of the ASPL emission has been used to quantify the temperature of CsPbBr₃ NCs during previous optical cooling studies. ¹

Importantly, E_a and ΔE are distinct energetic parameters that describe the ASPL process. ΔE is dependent only on the energy difference between the absorbed and emitted photon, while E_a is a measure of the intermediate step of the upconversion mechanism that requires the greatest quantity of thermal energy. An apt analogy can be made to chemical reaction kinetics, where ΔE is the difference in energies of the reactants and products, while E_a is defined by the rate limiting step, i.e., the most energetically costly step, of the reaction. By measuring how E_a correlates with ΔE , we gain some insight

into intermediate steps of the up-conversion process that may be missed by only looking at spectral indicators.

We measured ASPL intensity from colloidal suspensions of CsPbBr₃ NCs over a temperature range of 0 to 20 °C. The colloidal suspensions had a concentration of 0.20 μ M and a PLQY of 80%. The temperatures are plotted as ln(ASPL) versus (1/T), and the slope of best fit determines E_a , according to eq 1. This experiment was repeated as the excitation wavelength was detuned to lower energy, to probe the relationship between E_a and ΔE (see Figure 2B). A summary of this trend is displayed in Figure 2C. We note the E_a values reported here are significantly lower than $E_{\rm a}$ values at similar $\Delta E_{\rm s}$ that our laboratory reported previously. ^{1,31} In our earlier studies NCs were deposited as films encapsulated in polystyrene, while all measurements in this paper were performed on NCs in colloidal suspensions. These different environments apparently result in large changes to E_a . The experimentally measured E_a values are shown in blue with a dashed blue line indicating the line of best fit. Additionally, the hypothetical scenario when $E_a = \Delta E$ is also plotted using a dashed gray line. The activation energy is routinely greater than the corresponding ΔE , and the difference between the values increases as ΔE increases. The difference is clearly quantified by comparison of the line of best fit of the data with the gray $E_a = \Delta E$. The linear fits for E_a versus ΔE with varying excitation power densities is summarized in Table 1. A slight

Table 1. A Summary of the Linear Fits of E_a Versus ΔE for Multiple Excitation Power Densities

excitation power density (mW/cm²)	3.5	27	100
slope of linear fit of E_a vs ΔE (meV/meV)	1.4 ± 0.2	1.3 ± 0.1	1.2 ± 0.1
<i>y</i> -intercept of Linear fit of E_a vs ΔE (meV)	-4 ± 8	-3 ± 9	-5 ± 8

decrease in deviation from the hypothetical $E_{\rm a}=\Delta E$ scenario is observed as excitation power density increases and could be the result of a bottleneck effect or saturation of the lowest lying states mediating up-conversion. The growing discrepancy between $E_{\rm a}$ and ΔE indicates that there is significant energy cost for up-conversion in addition to ΔE , which increases as the energy gained from up-conversion increases.

Surface Polaron Sub-Gap States. The discrepancy and growing deviation between $E_{\rm a}$ and ΔE suggest that ASPL in CsPbBr₃ NCs is not the result of inelastic scattering from a phonon mode—e.g. an instantaneous Raman-like process—because no energy barrier would be expected in addition to the inelastic energy shift. Further, the large ΔE values that are greater than any phonon modes in the material, and the smooth exponential decrease in ASPL with red-shifted excitation, suggest that up-conversion is not the result of resonant absorption of a single phonon mode. Future time-resolved studies may be able to provide more insight into the time scales associated with the microscopic steps of ASPL, helping to further distinguish mechanisms.

The growing difference in energy between E_a and ΔE is indicative of MGP assisted ASPL and can be analyzed in terms of Marcus Theory. Marcus Theory was originally developed to describe electron transfer reactions in solution and has been extended to model the kinetics of carrier trapping and polaron behavior in semiconductor NCs. The theory considers how the movement of electrons between structurally distinct electronic states is associated with an additional energy cost that accounts for the atomic rearrangement. 43-45 In our experiments the difference in energy between E_a and ΔE suggests that ASPL is assisted by mid-gap polaron states (MPG) with an associated energy of rearrangement, E_R , when electrons move from the structurally distorted MGP state to the standard free exciton state (FE), as depicted schematically in Figure 3A. In the diagram each gray parabolic energy well corresponds to a distinct atomic configuration associated with a MGP state, with the energy of the electron in the MGP further modified as the atoms are displaced around their equilibrium positions. MGPs with lower electronic energy are associated with greater lattice distortion and are shifted more along the nuclear coordinate axis compared to the free exciton, FE, state. 46 As ΔE increases (corresponding to more red-shifted excitation), charge carriers are excited into MPGs at lower energy. Because of the greater structural distortion of MPG states at lower energy, more thermal energy is required for the atomic rearrangement when carriers move from the MPG to the FE. In other words, the increase in the apparent barrier height between the MPG and the FE reasonably explains the growing discrepancy between E_a and ΔE as ΔE increases. Given our interpretation, these data also give insight into the quantity of energy that is required to

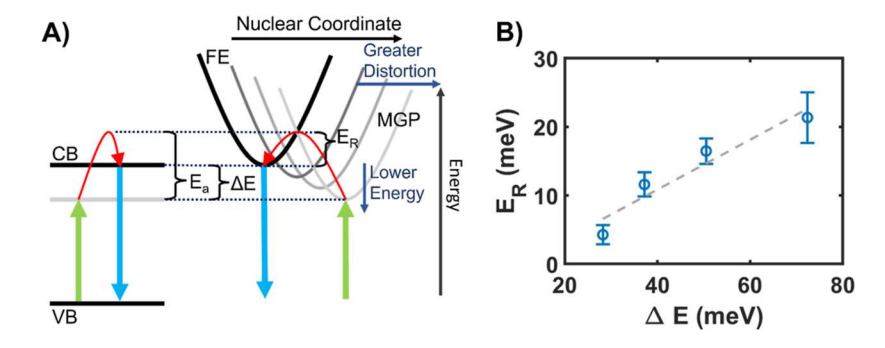


Figure 3. (A) Proposed model for ASPL in CsPbBr₃ NCs assisted by mid-gap polaron states. The difference between E_a and ΔE is the additional energy required for the atomic rearrangement (E_R) when moving between states. Sub-gap light excites charge carriers into an exponentially decreasing density of mid-gap polaron states (MGP), charge carriers are then thermally activated into the FE conduction band (CB) state, overcoming the energy barrier of E_a , followed by radiative relaxation to the ground state. E_R increases with ΔE because MGPs with lower electronic energy are more distorted along the nuclear coordinate compared to the FE state. (B) Plot of energy of rearrangement (E_R) versus up-conversion energy gain (ΔE) . The E_R values are calculated from measured E_a . The ΔE are shown in blue, the dashed gray line is the line of best fit.

rearrange the lattice, $E_{\rm R}$, during ASPL. The value of $E_{\rm R}$ is calculated by subtracting ΔE from $E_{\rm a}$. Figure 3B shows $E_{\rm R}$ values calculated using this method, compared to ΔE values. It can be noted that there is sufficient thermal energy at room temperature ($\sim\!2k_{\rm b}T$) to overcome the measured $E_{\rm R}$ values. We find it helpful to further analyze trends in terms of $E_{\rm R}$ going forward.

The prevalence of polarons in perovskites has been widely discussed, 35,46,47 and polarons have previously been proposed as assisting in CsPbBr₃ NC up-conversion. 22,32,33 Previous measurements have identified distortions of the PbBr₆ octahedral as being most often associated with polaron formation. 34,35,46 Though it is difficult to ascribe a single phonon mode to the up-conversion mechanism as the ΔEs which are attained are much greater than any single phononmode measured in CsPbBr3 NCs. Therefore, several researchers have proposed that up-conversion is the result of a multiphonon process.^{27,28} Prior studies have suggested that STEs are the particular class of MGP states that facilitate ASPL up-conversion in CsPbBr₃ NCs.²² STEs are localized distortions in the crystal lattice, induced by light, that stabilize bound excitons in ionic materials with strong electronphonon coupling. STEs are identified by their broad, redshifted emission spectra and can arise from material defects or inherent material properties. They have been detected across a broad range of halide perovskite materials. 22,43,46,48 Nonetheless, the formation of STEs typically depends on excitation energies larger than the band gap, which makes them improbable as the MGP states that promote ASPL in CsPbBr₃

Alternatively, we propose that the MGP states which assist in ASPL are likely formed spontaneously by thermal fluctuations in the crystal lattice either before or simultaneously with optical excitation. Lead halide perovskites are known to have a "soft", compliant lattice that readily undergoes thermal fluctuations that polarize and distort the atomic structure, especially the PbBr3 octahedral sub unit of the cell. 34,35,46 These transient, thermally induced distortions significantly modify the band edge electronic state structure, and the net result is a continuum of phonon-coupled electronic states that spectrally broaden the absorption edge near the band gap.^{32–36} We hypothesize that such transient, thermally induced MGP states may be stabilized by the occupation of a photocarrier in a manner that is analogous to how STE polaron states are stabilized by the presence of an exciton. Relatively long lifetimes for the states that mediate ASPL are required for thermal activation from MGP state to FE state to out-compete other recombination pathways. Research is ongoing in our laboratory to query the temperature dependence of the Urbach tail for insight into the formation and time scales of these states, as well as how they may impose bounds on the efficiency of optical cooling via ASPL.

Surface Environment and Ligand Coverage. The MGP states are expected to primarily form on the surface of NCs, because the motion of surface atoms is less constrained than that of atoms in the center of the lattice, making them more susceptible to lattice distortion and the formation of polaron states. This effect is widely acknowledged such that the red, broadband emission from STEs is sometimes simply referred to as surface emission. Likewise, thermal fluctuation induced MGPs are most prominent at the surface. Indeed, we find that modification of the surface environment of the NCs has a pronounced effect on E_R .

CsPbBr₃ NCs are capped with organic ligands during synthesis, which help control the growth of the NCs and act as passivating agents for surface defects, decreasing defect states that promote non-radiative recombination. ⁴⁹ Oleic acid and oleylamine are commonly used ligands that provide samples with very high PLQY, however these ligands only weakly bind to the surface of CsPbBr₃ NCs. Consequently, colloidal solutions of CsPbBr₃ NCs at low concentrations suffer from poor ligand coverage and low PLQY. Equilibration between surface-bound ligands and ligands that freely dissolve in the solvent phase favors unbound, freely dissolved ligands when NCs are at low concentrations. ^{49,50} The lower surface ligand coverage in more dilute NC suspensions was confirmed by performing NMR DOSY studies of the diffusion coefficient of the surface ligand (see Figure S8 and Table S2). Figure 4A

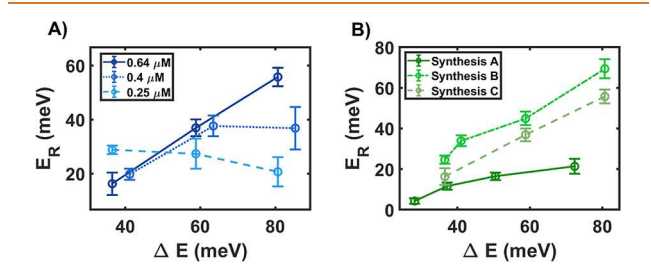


Figure 4. (A) $E_{\rm R}$ versus ΔE plot for different colloidal concentrations. (B) $E_{\rm R}$ versus ΔE plot for three different syntheses of varying concentrations and similar PLQYs. Synthesis A: concentration of 0.20 μ M, PLQY of 80%. Synthesis B: concentration of 0.64 μ M, PLQY of 81%. Synthesis C: concentration of 0.64 μ M, PLQY of 82%.

shows the effect of concentration on the relationship between $E_{\rm R}$ and ΔE . Three solutions of concentrations 0.64, 0.40, and 0.25 μ M, with PLQYs of 82, 78, and 70% respectively, were measured. Solutions with high colloidal concentrations, and therefore high ligand coverage, show a steep increase of $E_{\rm R}$ with ΔE . As NC concentration and ligand coverage decrease, the increase in $E_{\rm R}$ becomes less pronounced. At the lowest concentration, the trend is constant, or possibly reversed within our experimental resolution, with $E_{\rm R}$ weakly decreasing as ΔE increases. However, in general, at low colloidal concentrations PLQY decreases, because there is a lack of ligands to passivate defects. In samples with low PLQY, thermal activation of non-radiative recombination in parallel with ASPL could have an impact on the fitted trend determining $E_{\rm a}$.

In a separate experiment, three different NC samples were synthesized and purified to produce colloid suspension at different concentrations. However, all samples display PLQY of ~80% after dilution, with similar absorption and emission spectra. We note that there is stochastic variation in the PLQY of NCs from batch to batch, enabling this study. Synthesis A resulted in higher quality NCs and achieved a PLQY of 80% at a concentration of 0.20 μ M, while syntheses B and C were measured at a concentration of 0.64 μ M. As all three syntheses have the same PLQY, it can be assumed they all have a similar ratio of non-radiative recombination. Nonetheless, for purified samples, the desorption of surface-bound ligands is an equilibrium effect that is dictated by the overall concentration of NCs in the colloid suspension, so synthesis A had less surface-bound ligands and more solution-phase ligands. Figure 4B shows the trend in E_R for syntheses B and C. These samples

were measured at the same concentration, and we observe a very similar trend in $E_{\rm R}$ that increases with ΔE . In contrast synthesis A shows a less steep increase in $E_{\rm R}$. The behavior is consistent with what was observed in the study summarized in Figure 4A. Here again, we observe that greater ligand coverage increases the energetic cost of ASPL.

Returning to the physical picture in terms of Marcus Theory (see Figures 3 and S9), a change in $E_{\rm R}$ for the same ΔE indicates a change in the energetic cost for atomic displacements along the nuclear coordinated associated with the MGP state. A greater $E_{\rm R}$ value would imply a narrower parabola. That is, small atomic displacements have a large energy cost, indicating a less mechanically flexible structure. Conversely, a lower $E_{\rm R}$ value implies a shallower parabola associated with the MGP. In the latter case it is easier for thermal activation to move charge carriers from the MGP to the FE state, or equivalently to induce the required structural distortion.

We hypothesize that increased ligand coverage modifies the energetics of MGPs in such a way that atomic displacements become more energetically costly, i.e. the energetic parabola narrows. Samples with higher ligand coverage show a greater increase in E_R with ΔE , implying that high ligand coverage has a restrictive effect on MGPs, decreasing the magnitude of thermally induced structural distortions. Samples with lower ligand coverage likely have more flexible MGPs, because we do not observe as steep of an increase in E_R with ΔE . When low ligand coverage and poor PLQY are combined (as in the case with 0.25 μ M sample in Figure 4A) the $E_R/\Delta E$ relationship becomes more complicated and may result from more flexible MGPs as well as contributions from the thermal activation of non-radiative recombination. Alternatively the trend could be indicating the MGP-to-FE transition is in the "inverted region" described in Marcus Theory.⁵¹ Whether the relevant atomic rearrangement involves surface ligand rearrangement, ligand-NC bonds, or the crystal structure near the surface is unclear at this time.

CONCLUSION

In conclusion we quantified the Arrhenius behavior of ASPL in CsPbBr₃ NCs to probe how much thermal energy is required to promote optical up-conversion by an amount ΔE . We find that significantly more thermal energy is required than ΔE , and we hypothesize the additional energy cost is required for atomic rearrangement when photocarriers pass from mid-gap polaron (MGP) states to the FE state. That is, our data suggests that ASPL in CsPbBr3 NCs occurs via a MGP-assisted mechanism. Our interpretation is further supported by the larger energetic cost for ASPL when the NC surface ligand coverage is more robust, as the relevant MGPs likely form primarily on NC surfaces. We note that MGPs can be associated with surface sites, or within the bulk-like interior of NCs. Our data highlights how changes to surface environment modifies $E_{\rm R}$, suggesting the importance of MGPs at the NC surface. These findings suggest that surface ligand systems that preserve near-unity PLQY but that do not impede polaron formation may benefit the strategic design of CsPbBr3 NCs for optical cooling.

METHODS

<code>CsPbBr3</code> NC Synthesis and Characterization. The <code>CsPbBr3</code> NCs were synthesized using a hot-injection method adapted from procedures described by <code>Protesescu. 52 PbBr2</code> was heated in octadecene at 120 $^{\circ}$ C for 1 h to drive off impurities. <code>CsCO3</code> was

combined with oleic acid in octadecene and heated at 110 °C for 1 h to form Cs-oleate and drive off impurities. A 1:1 ratio of dried oleic acid and oleyl amine was added to the PbBr $_2$ solution which was then heated again. Cs-oleate was injected as the limiting reactant into the PbBr $_2$ solution at approximately 178 °C, after which the reaction flask was immediately cooled in an ice bath to quench the reaction. The reaction solution was then centrifuged for 10 min at 3000 rcf, the supernatant, containing the octadecene, was discarded. The precipitated NCs were dissolved in 2–4 mL of hexane and centrifuged again for 10 min at 3000 rcf, to remove the largest particles. The precipitate was discarded, and supernatant was treated with NH $_4$ SCN for approximately 30 min to reduce surface traps. No anti-solvents were used in the cleaning of the NCs.

Each batch was characterized using photoluminescence and absorbance spectroscopy at room temperature, using a DH-2000-BAL deuterium and halogen lamp and a Flame miniature spectrometer, both from Ocean Optics. Colloidal concentrations were calculated with Beer's Law using absorbance values at 335 nm and the molar extinction coefficient reported by De Roo et al. ⁵⁰

PLQY Measurement. PLQY measurements were taken at room temperature with an integrating sphere fitted with a monochromator and Si detector. A SuperK Fianium laser fitted with a LLTFContrast wavelength selector was used as an excitation source. The 470 nm excitation beam was chopped, and the signal was processed by a 830 Stanford Lock-in Amplifier. The whole system was calibrated for detection response. In order to correct for reabsorption, measurements of multiple samples with different concentrations were performed.⁵³

Arrhenius Measurement Experimental Set Up. CsPbBr₃ NCs were diluted to the desired concentration using hexane. The sample was prepared under inert atmosphere in a standard quartz cuvette with a magnetic stir bar. A bath of acetone and dry ice was used to cool down the sample and measurements were taken periodically as the sample and bath warmed up to room temperature, both sample and bath were stirred using magnetic stir bars to ensure thermal equilibrium. A digital thermometer in the bath was used to monitor the temperature. Lab gas was blown along the outsides of the temperature bath to prevent the formation of condensation that could interfere with measurements. Measurements were started when the bath temperature reached 0 °C and concluded when the bath reached room temperature, typical temperature range for measurements was between 0 and 18 °C. Joule heating of the sample is considered to be negligible due to the colloidal nature of the samples, the low excitation powers used and the low absorbance cross section in the probed region. A SuperK Fianum laser fitted with a LLTFContrast wavelength selector was used as an excitation source, the power density was controlled with a neutral density filter. A Flame miniature spectrometer from Ocean Optics was used to measure the ASPL spectra at different temperatures. We note the relatively low excitation powers used in comparison to other recent studies of ASPL in CsPbBr₃.³¹ The longer excitation path length (1 cm) through the sample, in combination with improved collection efficiency, allows for significantly lower overall excitation power to obtain sufficient signal-

Arrhenius Data Analysis and E_a **Calculation.** The high energy side of the spectra were fit to a Voigt function, to edit out the scattered excitation line. The Voigt function was integrated to get the ASPL intensity. The data was plotted on a $\ln(\text{ASPL})$ vs 1/T plot and a line of best fit was calculated for the data. Using the linear form of the Arrhenius equation $\ln(\text{ASPL}) = \frac{-E_a}{k_b} \left(\frac{1}{T}\right) + \ln(A)$, the slope of this line is equal to $\frac{-E_a}{k_b}$, and E_a can be easily calculated using Boltzmann's constant k_b . The reported uncertainty of the E_a values is the 95% confidence interval of the linear fit.

Absorbance and ΔE ASPL Measurements. Absorbance measurements were taken at room temperature with H-2000-BAL deuterium and halogen lamp and a Flame miniature spectrometer, with 25 μ m aperture, all purchased from Ocean Optics. ΔE dependent ASPL measurements were taken using a SuperK Fianum

laser fitted with a LLTFC ontrast wavelength selector and a Flame miniature spectrometer as a detector. A SPL intensity was calculated using a Voigt fit as described in the Arrhenius data and $E_{\rm a}$ calculation section.

ASSOCIATED CONTENT

5 Supporting Information

The Supporting Information is available free of charge at https://pubs.acs.org/doi/10.1021/acsnano.4c03548.

Sample TEM images of CsPbBr₃ NCs. Sample absorbance and photoluminescence spectra of CsPbBr₃ NCs. Anti-Stokes photoluminescence intensity versus power study. Comparison of photoluminescence peak position and Urbach energy. Comparison of Urbach tail and anti-Stokes photoluminescence intensity. Comparison of Stokes photoluminescence and anti-Stokes photoluminescence and anti-Stokes photoluminescence spectra. DOSY NMR ligand diffusion coefficient measurements. Marcus theory diagram of structurally flexible and inflexible mid-gap polarons (PDF)

AUTHOR INFORMATION

Corresponding Author

Matthew T. Sheldon — Department of Chemistry, Texas A&M University, College Station, Texas 77840-7896, United States; Department of Chemistry, University of California Irvine, Irvine, California 92697, United States; oorcid.org/0000-0002-4940-7966; Email: m.sheldon@uci.edu

Authors

Kylie M. Lytle – Department of Chemistry, Texas A&M University, College Station, Texas 77840-7896, United States; occid.org/0009-0006-3069-6805

Emma L. Brass – Department of Chemistry, University of California Irvine, Irvine, California 92697, United States

Benjamin J. Roman — Department of Chemistry, Texas A&M University, College Station, Texas 77840-7896, United States

Complete contact information is available at: https://pubs.acs.org/10.1021/acsnano.4c03548

Author Contributions

The manuscript was written through contributions of all authors. All authors have given approval to the final version of the manuscript.

Funding

This work was supported by the National Science Foundation (Grant No. DMR-2131408) and the Welch Foundation (A-1886).

Notes

The authors declare no competing financial interest.

REFERENCES

- (1) Roman, B. J.; Villegas, N. M.; Lytle, K.; Sheldon, M. Optically Cooling Cesium Lead Tribromide Nanocrystals. *Nano Lett.* **2020**, *20*, 8874–8879.
- (2) Epstein, R. I.; Buchwald, M. I.; Edwards, B. C.; Gosnell, T. R.; Mungan, C. E. Observation of laser-induced fluorescent cooling of a solid. *Nature* **1995**, *377*, 500–503.
- (3) Hehlen, M. P.; Meng, J.; Albrecht, A. R.; Lee, E. R.; Gragossian, A.; Love, S. P.; Hamilton, C. E.; Epstein, R. I.; Sheik-Bahae, M. First demonstration of an all-solid-state optical cryocooler. *Light Sci. Appl.* **2018**, *7*, 15.

- (4) Melgaard, S. D.; Albrecht, A. R.; Hehlen, M. P.; Sheik-Bahae, M. Solid-state optical refrigeration to sub-100 Kelvin regime. *Sci. Rep.* **2016**, *6*, 20380.
- (5) Bartholomew, J. L.; DeBarber, P. A.; Heeg, B.; Rumbles, G. Development of an organic dye solution for laser cooling by anti-Stokes fluorescence. MRS Online Proc. Lib. 2001, 667, 17.
- (6) Dimitriev, O.; Fedoryak, A.; Slominskii, Y.; Smirnova, A.; Yoshida, T. Phonon-assisted anti-Stokes luminescence of tricarbocyanine near-infrared dye. *Chem. Phys. Lett.* **2020**, 738, 136905.
- (7) Clark, J. L.; Miller, P. F.; Rumbles, G. Red Edge Photophysics of Ethanolic Rhodamine 101 and the Observation of Laser Cooling in the Condensed Phase. *J. Phys. Chem. A* **1998**, *102*, 4428–4437.
- (8) Zhang, J.; Li, D.; Chen, R.; Xiong, Q. Laser cooling of a semiconductor by 40 K. Nature 2013, 493, 504-508.
- (9) Ha, S.-T.; Shen, C.; Zhang, J.; Xiong, Q. Laser cooling of organic-inorganic lead halide perovskites. *Nat. Photonics* **2016**, *10*, 115–121.
- (10) Clark, J. L.; Rumbles, G. Laser Cooling in the Condensed Phase by Frequency Up-Conversion. *Phys. Rev. Lett.* **1996**, 76, 2037—2040.
- (11) Finkeißen, E.; Potemski, M.; Wyder, P.; Viña, L.; Weimann, G. Cooling of a semiconductor by luminescence up-conversion. *Appl. Phys. Lett.* **1999**, *75*, 1258–1260.
- (12) Morozov, Y. V.; Zhang, S.; Pant, A.; Jankó, B.; Melgaard, S. D.; Bender, D. A.; Pauzauskie, P. J.; Kuno, M. Can lasers really refrigerate CdS nanobelts? *Nature* **2019**, *570*, E60–E61.
- (13) Zhang, J.; Li, D.; Xiong, Q. Reply to: Can lasers really refrigerate CdS nanobelts? *Nature* **2019**, *570*, E62–E64.
- (14) Mungan, C. E.; Gosnell, T. R. Comment on Laser Cooling in the Condensed Phase by Frequency Up-Conversion". *Phys. Rev. Lett.* **1996**, 77, 2840.
- (15) Michael, P. H.; Mansoor, S.-B.; Richard, I. E. Effect of high carrier density on luminescence thermometry in semiconductors. In *Proceedings SPIE 6461, Laser Cooling of Solids*; SPIE, 2007, p 646107...
- (16) Seletskiy, D. V.; Melgaard, S. D.; Di Lieto, A.; Tonelli, M.; Sheik-Bahae, M. Laser cooling of a semiconductor load to 165 K. *Opt. Express* **2010**, *18*, 18061.
- (17) Oraevsky, A. N. Cooling of semiconductors by laser radiation. *Quantum Electron.* **1996**, 26, 1018–1022.
- (18) Rivlin, L. A.; Zadernovsky, A. A. Laser cooling of semi-conductors. *Opt. Commun.* 1997, 139, 219–222.
- (19) Sheik-Bahae, M.; Epstein, R. I. Can laser light cool semiconductors? *Phys. Rev. Lett.* **2004**, 92, 247403.
- (20) Khurgin, J. B. Role of bandtail states in laser cooling of semiconductors. *Phys. Rev. B* **2008**, *77*, 235206.
- (21) Khurgin, J. B. Band gap engineering for laser cooling of semiconductors. *J. Appl. Phys.* **2006**, *100*, 113116.
- (22) Ma, X.; Pan, F.; Li, H.; Shen, P.; Ma, C.; Zhang, L.; Niu, H.; Zhu, Y.; Xu, S.; Ye, H. Mechanism of Single-Photon Upconversion Photoluminescence in All-Inorganic Perovskite Nanocrystals: The Role of Self-Trapped Excitons. *J. Phys. Chem. Lett.* **2019**, *10*, 5989–5996.
- (23) Li, X.; Cao, F.; Yu, D.; Chen, J.; Sun, Z.; Shen, Y.; Zhu, Y.; Wang, L.; Wei, Y.; Wu, Y.; Zeng, H. All Inorganic Halide Perovskites Nanosystem: Synthesis, Structural Features, Optical Properties and Optoelectronic Applications. *Small* **2017**, *13*, 1603996.
- (24) Koscher, B. A.; Swabeck, J. K.; Bronstein, N. D.; Alivisatos, A. P. Essentially Trap-Free CsPbBr3 Colloidal Nanocrystals by Postsynthetic Thiocyanate Surface Treatment. J. Am. Chem. Soc. 2017, 139, 6566–6569.
- (25) Roman, B. J.; Sheldon, M. T. Six-fold plasmonic enhancement of thermal scavenging via CsPbBr3 anti-Stokes photoluminescence. *Nanophotonics* **2019**, *8*, 599–605.
- (26) Pokryshkin, N. S.; Mantsevich, V. N.; Timoshenko, V. Y. Anti-Stokes Photoluminescence in Halide Perovskite Nanocrystals: From Understanding the Mechanism towards Application in Fully Solid-State Optical Cooling. *Nanomaterials* **2023**, *13*, 1833.
- (27) Zhang, Z.; Ghonge, S.; Ding, Y.; Zhang, S.; Berciu, M.; Schaller, R. D.; Jankó, B.; Kuno, M. Resonant Multiple-Phonon Absorption

- Causes Efficient Anti-Stokes Photoluminescence in CsPbBr3 Nanocrystals. ACS Nano 2024, 18, 6438-6444.
- (28) Águila, A. G. d.; Do, T. T. H.; Xing, J.; Jee, W. J.; Khurgin, J. B.; Xiong, Q. Efficient up-conversion photoluminescence in all-inorganic lead halide perovskite nanocrystals. *Nano Res.* **2020**, *13*, 1962–1969.
- (29) Morozov, Y. V.; Draguta, S.; Zhang, S.; Cadranel, A.; Wang, Y.; Janko, B.; Kuno, M. Defect-Mediated CdS Nanobelt Photoluminescence Up-Conversion. *J. Phys. Chem. C* **2017**, *121*, 16607–16616.
- (30) Ye, S.; Zhao, M.; Yu, M.; Zhu, M.; Yan, W.; Song, J.; Qu, J. Mechanistic Investigation of Upconversion Photoluminescence in All-Inorganic Perovskite CsPbBrI2 Nanocrystals. *J. Phys. Chem. C* **2018**, 122, 3152–3156.
- (31) Roman, B.; Sheldon, M. The role of mid-gap states in allinorganic CsPbBr3 nanoparticle one photon up-conversion. *Chem. Commun.* **2018**, *54*, *6851*–*6854*.
- (32) Zhang, W.; Ye, Y.; Liu, C.; Wang, J.; Ruan, J.; Zhao, X.; Han, J. Two-Step Anti-Stokes Photoluminescence of CsPbX3 Nanocrystals. *Adv. Opt. Mater.* **2021**, *9*, 2001885.
- (33) Wu, B.; Wang, A.; Fu, J.; Zhang, Y.; Yang, C.; Gong, Y.; Jiang, C.; Long, M.; Zhou, G.; Yue, S.; et al. Uncovering the mechanisms of efficient upconversion in two-dimensional perovskites with anti-Stokes shift up to 220 meV. *Sci. Adv.* **2023**, *9*, No. eadi9347.
- (34) Wu, B.; Yuan, H.; Xu, Q.; Steele, J. A.; Giovanni, D.; Puech, P.; Fu, J.; Ng, Y. F.; Jamaludin, N. F.; Solanki, A.; et al. Indirect tail states formation by thermal-induced polar fluctuations in halide perovskites. *Nat. Commun.* **2019**, *10*, 484.
- (35) Yaffe, O.; Guo, Y.; Tan, L. Z.; Egger, D. A.; Hull, T.; Stoumpos, C. C.; Zheng, F.; Heinz, T. F.; Kronik, L.; Kanatzidis, M. G.; et al. Local Polar Fluctuations in Lead Halide Perovskite Crystals. *Phys. Rev. Lett.* **2017**, *118*, 136001.
- (36) Lanigan-Atkins, T.; He, X.; Krogstad, M. J.; Pajerowski, D. M.; Abernathy, D. L.; Xu, G. N. M. N.; Xu, Z.; Chung, D. Y.; Kanatzidis, M. G.; Rosenkranz, S.; et al. Two-dimensional overdamped fluctuations of the soft perovskite lattice in CsPbBr3. *Nat. Mater.* **2021**, 20 (7), 977–983.
- (37) Morozov, Y. V.; Zhang, S.; Brennan, M. C.; Janko, B.; Kuno, M. Photoluminescence Up-Conversion in CsPbBr3 Nanocrystals. *ACS Energy Lett.* **2017**, *2*, 2514–2515.
- (38) Studenyak, I.; Kranjčec, M.; Kurik, M. Urbach Rule in Solid State Physics. *Int. J. Opt. Appl.* **2014**, *4*, 76–83.
- (39) Ledinsky, M.; Schönfeldová, T.; Holovský, J.; Aydin, E.; Hájková, Z.; Landová, L.; Neyková, N.; Fejfar, A.; De Wolf, S. Temperature Dependence of the Urbach Energy in Lead Iodide Perovskites. *I. Phys. Chem. Lett.* **2019**, *10*, 1368–1373.
- (40) Guyot-Sionnest, P.; Lhuillier, E.; Liu, H. A mirage study of CdSe colloidal quantum dot films, Urbach tail, and surface states. *J. Chem. Phys.* **2012**, *137*, 154704.
- (41) Cheng, O. H.-C.; Qiao, T.; Sheldon, M.; Son, D. H. Size- and temperature-dependent photoluminescence spectra of strongly confined CsPbBr3 quantum dots. *Nanoscale* **2020**, *12*, 13113–13118.
- (42) Raiò, G.; Becker, M. A.; Bodnarchuk, M. I.; Mahrt, R. F.; Kovalenko, M. V.; Stöferle, T. Superfluorescence from lead halide perovskite quantum dot superlattices. *Nature* **2018**, *563*, *671*–*675*.
- (43) Mack, T. G.; Jethi, L.; Kambhampati, P. Strategy for Exploiting Self-Trapped Excitons in Semiconductor Nanocrystals for White Light Generation. ACS Photonics 2019, 6, 1118–1124.
- (44) Mooney, J.; Krause, M. M.; Saari, J. I.; Kambhampati, P. Challenge to the deep-trap model of the surface in semiconductor nanocrystals. *Phys. Rev. B* **2013**, *87*, 081201.
- (45) Jones, M.; Lo, S. S.; Scholes, G. D. Quantitative modeling of the role of surface traps in CdSe/CdS/ZnS nanocrystal photoluminescence decay dynamics. *Proc. Natl. Acad. Sci. U.S.A.* **2009**, *106*, 3011–3016.
- (46) Xu, Z.; Jiang, X.; Cai, H.-p.; Chen, K.; Yao, X.; Feng, Y. Toward a General Understanding of Exciton Self-Trapping in Metal Halide Perovskites. *J. Phys.l Chem. Lett.* **2021**, *12*, 10472–10478.

- (47) Ghosh, D.; Welch, E.; Neukirch, A. J.; Zakhidov, A.; Tretiak, S. Polarons in Halide Perovskites: A Perspective. *J. Phys. Chem. Lett.* **2020**, 11, 3271–3286.
- (48) Li, S.; Luo, J.; Liu, J.; Tang, J. Self-Trapped Excitons in All-Inorganic Halide Perovskites: Fundamentals, Status, and Potential Applications. *J. Phys. Chem. Lett.* **2019**, *10*, 1999–2007.
- (49) Nenon, D. P.; Pressler, K.; Kang, J.; Koscher, B. A.; Olshansky, J. H.; Osowiecki, W. T.; Koc, M. A.; Wang, L.-W.; Alivisatos, A. P. Design Principles for Trap-Free CsPbX3 Nanocrystals: Enumerating and Eliminating Surface Halide Vacancies with Softer Lewis Bases. J. Am. Chem. Soc. 2018, 140, 17760–17772.
- (50) De Roo, J.; Ibáñez, M.; Geiregat, P.; Nedelcu, G.; Walravens, W.; Maes, J.; Martins, J. C.; Van Driessche, I.; Kovalenko, M. V.; Hens, Z. Highly Dynamic Ligand Binding and Light Absorption Coefficient of Cesium Lead Bromide Perovskite Nanocrystals. *ACS Nano* **2016**, *10*, 2071–2081.
- (51) Wang, J.; Ding, T.; Gao, K.; Wang, L.; Zhou, P.; Wu, K. Marcus inverted region of charge transfer from low-dimensional semi-conductor materials. *Nat. Commun.* **2021**, *12*, 6333.
- (52) Protesescu, L.; Yakunin, S.; Bodnarchuk, M. I.; Krieg, F.; Caputo, R.; Hendon, C. H.; Yang, R. X.; Walsh, A.; Kovalenko, M. V. Nanocrystals of Cesium Lead Halide Perovskites (CsPbX3, X = Cl, Br, and I): Novel Optoelectronic Materials Showing Bright Emission with Wide Color Gamut. *Nano Lett.* **2015**, *15*, 3692–3696.
- (53) Ahn, T.-S.; Al-Kaysi, R. O.; Müller, A. M.; Wentz, K. M.; Bardeen, C. J. Self-absorption correction for solid-state photoluminescence quantum yields obtained from integrating sphere measurements. *Rev. Sci. Instrum.* **2007**, *78*, 086105.